Transmission FT-IR and Knudsen Cell Study of the Heterogeneous Reactivity of Gaseous Nitrogen Dioxide on Mineral Oxide Particles

G. M. Underwood, T. M. Miller, and V. H. Grassian*

Department of Chemistry, University of Iowa, Iowa City, Iowa 52242

Received: May 14, 1999

The heterogeneous reactivity of gaseous nitrogen dioxide on mineral oxide particles was investigated. In particular, spectroscopic and kinetic measurements have been made to investigate surface reactions of NO_2 on Al_2O_3, Fe_2O_3, and TiO_2 at 298 K. Both gas-phase and surface-bound products are formed from the reaction of NO_2 with these mineral oxide particles. At low coverages, FT-IR spectra of the mineral oxide surface exposed to gaseous NO_2 show absorptions due to surface nitrite, specifically a chelating nitrito species. As the coverage increases, the surface becomes populated with surface nitrate bonded in several different bonding coordinations (monodentate, bidentate, and bridging). The predominant gas-phase product is NO, although there is a small amount (<1%) of detectable N_2O. A Knudsen cell reactor coupled to a quadrupole mass spectrometer was used to measure the uptake coefficient, γ, for NO_2 on these oxide particles and to characterize gas-phase product formation. The Knudsen cell data showed NO to be the major gas-phase product with a delay in the onset of NO production. There was little production of N_2O and no gas-phase HONO or HNO_3 was detected. By monitoring the reaction until completion, the ratio of NO_2 reacted to NO produced was determined to be ~2:1. These results complement the FT-IR data and suggest a two-step mechanism in which NO_2(g) is initially adsorbed as a nitrite species which subsequently reacts with additional NO_2 to form surface nitrate and gas-phase NO. Finally, the initial uptake coefficient was determined from the Knudsen cell data for NO_2 on Al_2O_3, Fe_2O_3, and TiO_2. Because NO_2 can diffuse into the underlying layers of these oxide particles, the use of a geometric area does not give accurate values of the uptake coefficient. Gas diffusion must be taken into account to more accurately determine the uptake coefficient.

Introduction

Nitrogen oxides are a major component of air pollution, and their chemical reactivity is of great importance in atmospheric chemistry.[1] Heterogeneous reactions that can alter NO_x ($NO_x = NO + NO_2$) concentrations have important implications for tropospheric ozone formation as ozone is not directly emitted into the troposphere, but is formed by a complex series of photochemical reactions involving nonlinear interactions among NO_x, volatile organic compounds (VOCs), and carbon monoxide.[2] Additionally, present models which rely on gas-phase chemical processes alone typically over-predict the HNO_3 to NO_x ratio by a factor of 5 to 10.[3,4] Heterogeneous processes that perturb NO_x or HNO_3 concentrations could potentially reconcile the predictions with the observations.

In general, kinetic and spectroscopic data are needed from laboratory studies of heterogeneous reactions in order to quantify reaction rates and determine reaction mechanisms for potentially important atmospheric reactions. There have been several laboratory studies of heterogeneous reactions of nitrogen oxides on the surface of a variety of atmospherically relevant particles, such as soot,[5−11] NaCl,[12−17] and fly,ash.[18] In the case of nitrogen dioxide, it has been shown that NO_2 can undergo heterogeneous reactions to form adsorbed products, such as surface nitrate,[12−18] and may evolve some other species in the gas phase, such as NO or HONO.[5−11] Because NO_2 can undergo reactions on surfaces to yield both surface-bound and gas-phase products, it is important to have analytical techniques that probe both adsorbed and gas-phase species. This dual observation of the surface and gas phase allows the mechanistic details of adsorption and surface reactions to be discerned.

In this study, the heterogeneous reactivity of NO_2 on three representative mineral oxides, Al_2O_3, Fe_2O_3, and TiO_2, is investigated. The work is motivated by the recent proposal that mineral aerosol may act as a reactive surface in the global troposphere.[19−22] Here we characterize surface-bound and gas-phase products, measure the uptake coefficients, and quantify both reactant and products for the heterogeneous reaction of NO_2 on these mineral oxides at 298 K. Transmission FT-IR spectroscopy is used to probe surface reactions of NO_2 on Al_2O_3, Fe_2O_3, and TiO_2 particles. The design of the experimental apparatus is such that FT-IR measurements of both the gas phase and surface species can be made. These laboratory measurements were performed on particles that are smaller than the mineral dust particles found in the atmosphere because high surface area particles are ideally suited for spectroscopic investigation of surface reactions. Using a Knudsen cell reactor coupled to a mass spectrometer, the uptake coefficients, γ, for NO_2 on Al_2O_3, Fe_2O_3, and TiO_2 were measured and the production of gas-phase species was quantified. In determining the uptake coefficients, the use of the geometric sample area was not justified and diffusion of NO_2 into the underlying layers needed to be considered to obtain more accuate values of γ.

Experimental Section

The IR cell used in this study has been described in detail before.[23,24] Briefly, the IR cell consists of a cube with two

* To whom correspondence should be addressed.

10.1021/jp991586i CCC: $18.00
Published on Web 07/14/1999

differentially pumped BaF_2 windows and a sample holder. A tungsten grid that is half coated with the mineral oxide is held in place by a set of Ni jaws mounted to Ni feedthroughs. This assembly can be used to resistively heat the sample. The temperature is monitored by a thermocouple spot-welded to the center of the tungsten grid. The IR cell is attached to a vacuum chamber through a flexible bellows hose. The vacuum chamber consists of an 80 L/s ion pump, a gas manifold, and two absolute pressure transducers for accurate pressure measurements (range from 1 to 1000 mTorr and 1 to 1000 Torr).

The infrared cell was mounted on a linear translator inside the FT-IR spectrometer so that both halves of the grid could be measured by simply moving the infrared cell through the IR beam path. Infrared spectra were recorded with a Mattson RS-10000 equipped with a narrowband MCT detector. Typically, 250 scans were collected with an instrument resolution of 4 cm^{-1} in the spectral range extending from 750 to 4000 cm^{-1}. Absorbance spectra for gas-phase and adsorbed species were obtained by referencing single-beam spectra of the blank grid and the mineral oxide-coated grid to single-beam spectra collected just prior to the first NO_2 exposure.

With the exception of the FT-IR experiments on Fe_2O_3, oxide particles were purchased from commercial sources. γ-Al_2O_3 (Alumina C, Degussa), α-Fe_2O_3 (Alfa Aesar), and TiO_2 (80% anatase, 20% rutile; P25 Degussa) particles with BET measured surface areas of 99, 2.3, and 52 m^2/g, respectively, were used in these experiments. The particles are nearly spherical with average particle diameters of 18 nm (Al_2O_3), 0.69 μm (Fe_2O_3), and 25 nm (TiO_2), as measured by transmission electron microscopy. Although the small particles can form larger aggregates, on the order of 500 nm, we did not observe this effect using the sample preparation techniques outlined below.[25]

For the FT-IR experiments, Al_2O_2 and TiO_2 samples were prepared by spraying a slurry of the oxide powder onto half of a tungsten grid. The other half of the grid was left blank so that gas-phase measurements could be made. Sample weights of approximately 36 mg for Al_2O_3 and 45 mg for TiO_2 were sprayed onto a 3 cm $\times$ 1 cm area of the tungsten grid. The grid was then mounted inside the IR cell and pumped by a turbomolecular pump to a pressure of 1×10^{-6} Torr.

For IR measurements, higher surface area iron oxide particles were prepared from iron hydroxide (α-FeOOH, Alfa Aesar). Approximately 14 mg of iron hydroxide were pressed onto half of a tungsten grid, again leaving the other half blank. The sample was heated in the IR cell to 523 K under vacuum overnight and subsequently oxidized for 60 min at 673 K followed by evacuation. This procedure converts α-FeOOH particles to α-Fe_2O_3 particles with a BET surface area of 96 m^2/g.

A Knudsen cell reactor coupled to a quadrupole mass spectrometer (UTI, DetecTorr II) was used to quantify gas-phase product formation and to determine the uptake coefficients of NO_2 on the mineral oxide surfaces. The mass spectrometer is housed in a vacuum chamber equipped with a 400 L/s ion pump and an ion gauge (both from Varian). The region between the quadrupole mass spectrometer and the Knudsen cell reactor is pumped by a 150 L/s turbomolecular pump (Leybold) for differential pumping of the mass spectrometer.

The Knudsen cell reactor consists of a stainless steel reducing cross with a sample holder attached to the bottom flange. All exposed interior surfaces are coated with Halocarbon Wax series 1500 to provide a chemically inert surface. A blank flange attached to a linear translator serves as a cover for the powdered sample. The seal between the sample holder and the cover is made with a viton O-ring.

The cell volume and escape constant were determined by monitoring the pressure in the cell as a function of time after steady-state flow into the cell was abruptly stopped. For these experiments, the natural log of the relative pressure as a function of time yields a slope equal to the negative of k_{esc}. This value can in turn be used to determine the cell volume through the equation

$$k_{esc} = \left(\frac{\upsilon A_{H,eff}}{4V}\right) \quad (1)$$

where υ is the average gas-phase velocity, $A_{H,eff}$ is the effective area of the escape aperture accounting for the Clausing factor, and V is the volume of the cell. Using an aperture of 0.0204 cm^2 with a Clausing factor of 0.4726,[26] we found the escape constant and cell volume to be 0.12 s^{-1} and 765 cm^3, respectively.

Oxide samples for the Knudsen cell were prepared in one of two ways depending on the experiment. To measure the uptake coefficient, relatively large amounts of oxide (0.5−2.0 g) were used to ensure we were on the plateau of the pore diffusion model (see Discussion). For these experiments the powdered oxide was spread evenly across the sample holder, then lightly pressed down to form a flat surface. To quantify the total amount of reactants and products much less sample, 20−100 mg for the high surface area oxides and 200−500 mg for the iron oxide, was used. The use of less sample allowed the reaction to be followed to completion in a reasonable time period, typically a few hours. To ensure even coverage across the bottom of the sample holder for the high surface area oxides, alumina and titania, the oxide powder was sprayed onto the sample holder using the same technique described for the FT-IR experiments. This procedure yielded very even coverage as determined with an optical microscope.

For all of the Knudsen cell experiments, the reactor was passivated by flowing NO_2 through the reactor for at least 90 min prior to the experiment. NO_2 was introduced through a leak valve. During passivation the mineral oxide particles were sealed with the blank flange. At the beginning of the passivation process, the ratio of *m*/*e* 46 to *m*/*e* 30 was near 2.9. During the 90 min of passivation, the ratio typically changed by 6% until it reached a final value of 3.1. The pressure in the Knudsen cell was measured with an absolute pressure transducer (MKS 690A.1TRC range $1 \times 10^{-6} - 0.1$ Torr). The steady-state NO_2 concentration in the cell varied from $\sim 3 \times 10^{11}$ cm^{-3} (0.01 mT, 10 ppb) to $\sim 3 \times 10^{14}$ cm^{-3} (8 mT, 10 ppm).

Using simple gas kinetic theory combined with the experimentally determined cell parameters defined above and absolute pressure vs mass spectral intensity data, the NO_2 mass spectrometer signal was converted to molecular flow through the cell. Because the absolute pressure vs mass spectral intensity data was sensitive to fluctuations in the relative pumping speeds of the turbo and ion pumps, daily calibrations were made using NO_2. Relative mass spectral sensitivities for NO, N_2O, and NO_2 were determined from a calibration of the pure gases. These sensitivity factors were then used in conjunction with the daily NO_2 calibration to convert the mass spectrometer signal to molecular flow for NO and N_2O. Gaseous NO_2 (Matheson, 99.95% minimum purity), NO (Matheson, 99%), N_2O (Matheson, 99.9%), and O_2 (Air products, 99.6% minimum purity) were used as received.

Results

A. FT-IR Spectroscopy of NO_2 Adsorption on Al_2O_3, Fe_2O_3, and TiO_2. It is well-known that NO_2 and NO can react

TABLE 1: Assignment of Vibrational Bands of Adsorbed Nitrogen Oxides on Al_2O_3, Fe_2O_3, and TiO_2 from NO_2 Adsorption

Surface Species	Representation	Assignment	Al_2O_3	Fe_2O_3	TiO_2
Monodentate Nitrate	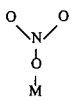	ν_3 low ν_3 high	a 1565 / 1532	1275 1556	1283 1510
Bidentate Nitrate		ν_3 low ν_3 high	a 1587	1250 1582	1238 1584
Bridging Nitrate		ν_3 low ν_3 high	a 1625	1225 1615	1230 1637
Solvated Nitrate	NO_3^- (aq)	ν_3 low ν_3 high	1302 1411	1305[b] c	1303[b] 1435[b]
Bidentate Nitrito		ν_3 ν_1	1230 1313	1192 1272	1178 1286

[a] Bands hidden under solvated nitrate absorption. [b] Observed only when water (~5% RH) is introduced into the IR cell.[49] [c] High-frequency band not observed.

on metal oxide surfaces to yield a number of different surface species that in principle can be differentiated by infrared spectroscopy. Nitrogen dioxide adsorption can result in the formation of both adsorbed nitrate (NO_3^-) and nitrite (NO_2^-).[27−32] The coordination of nitrate, nitrite, and nitric oxide in inorganic complexes has been discussed in the literature in some detail and provides a useful guide for the interpretation of the infrared absorption bands of adsorbed species.[33−35]

The FT-IR spectra of Al_2O_3, Fe_2O_3, and TiO_2 following exposure to NO_2 in the pressure range of 5−350 mTorr are shown in Figure 1. The spectra were recorded after evacuation of gas-phase NO_2. Single-beam spectra of the surface after exposure to NO_2 were referenced to single-beam spectra of the clean oxide prior to NO_2 adsorption. At the lowest pressures, features are apparent in the spectra which can be assigned to a chelating nitrite surface species, specifically a bidentate nitrito species (see Table 1).[34] These bands grow in intensity as the NO_2 pressure is increased to approximately 30 mTorr. Besides the increase in intensity of the nitrite bands with NO_2 pressure, several new bands become evident in the 1650−1150 cm^{-1} region as the NO_2 pressure increases. These new absorption bands can be assigned to the degenerate ν_3 mode of oxide-coordinated monodentate, bidentate, and bridging nitrate which has been split into two bands due to a loss of symmetry upon adsorption.[27−32,34,36] In the case of Al_2O_3, absorptions due to water-solvated surface nitrate at 1411 and 1302 cm^{-1} are also apparent. The presence of water-solvated nitrate on Al_2O_3 has been discussed previously.[37] Although the bands due to water-solvated nitrate and oxide-coordinated nitrate overlap in the 1302 cm^{-1} region, in previous experiments on heated samples of Al_2O_3 adsorbed water could be removed from the surface and the lower energy split of the ν_3 nitrate mode of the oxide-coordinated monodentate, bidentate, and bridging nitrate species could be clearly delineated.[24,37]

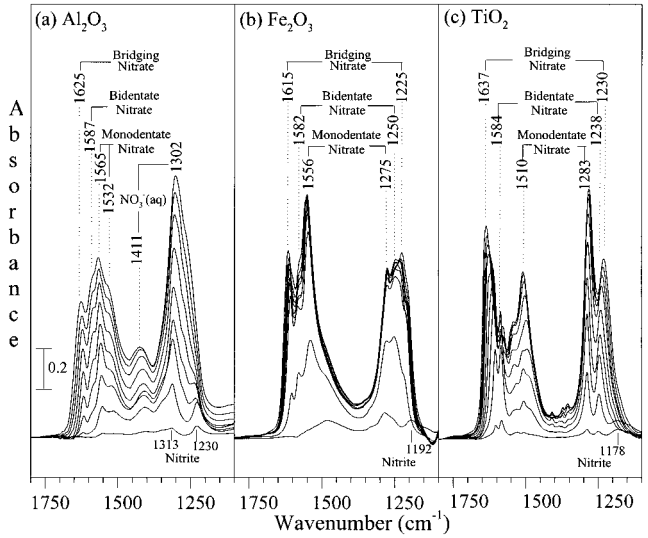

Figure 1. Transmission FT-IR spectra of (a) Al_2O_3, (b) Fe_2O_3, and (c) TiO_2 after exposure to NO_2. The spectra were recorded after evacuation of the gas phase following exposure of the oxides to NO_2 in the pressure range 5−350 mTorr. As discussed in the text, the absorption features indicate a conversion of nitrite to nitrate as coverage increases.

Surface-bound species are not the only products that form from the reaction of NO_2 with mineral oxide surfaces. For each pressure to which the oxides were exposed, FT-IR spectra of the gas phase were also taken. The spectra of the gas phase in the region extending from 1800−2300 cm^{-1} at a pressure of approximately 300 mTorr are shown in Figure 2. The gas-phase infrared data show that significant amounts of NO and, in the case of alumina, some N_2O are present in the IR cell. No other gas-phase products were detected. As measured in our laboratory, the extinction coefficient of N_2O is approximately twenty

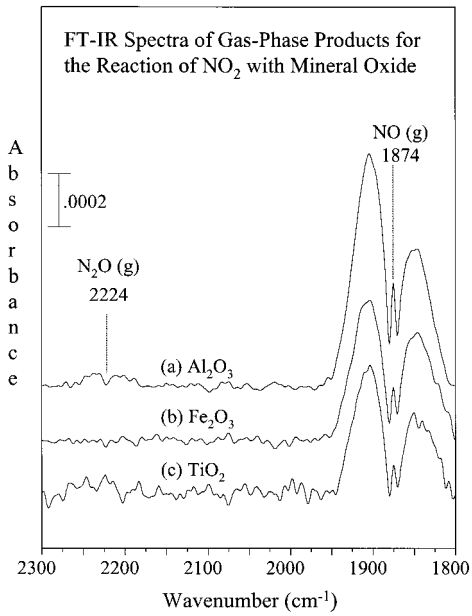

Figure 2. Transmission FT-IR spectra of the gas-phase products formed from reaction of NO_2 with (a) Al_2O_3, (b) Fe_2O_3, and (c) TiO_2 at an ambient pressure near 300 mTorr. Two gas-phase products are present: NO at 1874 cm^{-1} and N_2O at 2224 cm^{-1}.

times greater than that of NO. From this we estimate that N_2O accounts for less than 1% of the gas-phase products, even for alumina. Experiments where NO_2 was added to the FT-IR cell in the absence of mineral oxides also show some NO and N_2O formation; however, the amount formed is much less than when the mineral oxide particles are present. These control experiments show that wall reactions do occur, but account only for a small fraction of the gas-phase products. Because of these small but nonnegligible wall reactions and the large disparity in extinction coefficients, it is difficult to quantify the amount of NO and N_2O from the infrared data. However, experiments done in the Knudsen cell reactor can be used to quantify product formation (vide infra).

B. Knudsen Cell Reactor Measurements for NO_2 on Al_2O_3, Fe_2O_3, and TiO_2. Kinetic measurements of the heterogeneous reactivity of NO_2 on Al_2O_3, Fe_2O_3, and TiO_2 were made with a Knudsen cell reactor coupled to a quadrupole mass spectrometer. These measurements were used to quantify the production of gas-phase species and to determine the uptake coefficient, γ. The design of the Knudsen cell is such that the volume of the cell changes very little, <1%, when the sample compartment is opened to expose the mineral oxide particles. Therefore, no volume corrections are needed and the uptake coefficient, γ, is usually determined from eq 1:[12,38]

$$\gamma_g = \frac{A_{H,eff}}{A_s}\left(\frac{I_o - I_r}{I_r}\right) = \frac{A_{H,eff}}{A_s}\left(\frac{F_o - F_r}{F_r}\right) \qquad (2)$$

where γ_g is the calculated uptake coefficient using the geometric area, $A_{H,eff}$ is the effective geometric area of the escape aperture as described in the Experimental Section, and A_s is the geometric area of the sample holder, 11.88 cm^2. I_o is the mass spectrometer signal for the reactive gas prior to opening the sample compartment, and I_r is the mass spectrometer signal when the mineral oxide particles are exposed. Alternatively, as done here, the mass spectrometer signal can be calibrated (see Experimental Section) for flow rate of NO_2 in the presence, F_r, and absence, F_o, of the exposed reactive mineral oxide surface.

Typical Knudsen cell data used to determine the uptake coefficient for heterogeneous reaction of NO_2 on Al_2O_3, Fe_2O_3, and TiO_2 are shown in Figure 3. Initially, a steady-state flow of NO_2 is established, then the sample holder is opened and the NO_2 signal (*m*/*e* 46) drops below the steady-state value obtained before the mineral oxide particles were exposed. The sample holder is then closed periodically to check for drift in the baseline. During these times the NO_2 flow rate returns to its original steady-state value. The uptake coefficients that are reported in Figure 3 were determined using eq 1 and the parameters given in the Experimental Section. The values reported, 0.0002, 0.0012, and 0.0004, for Al_2O_3, Fe_2O_3, and TiO_2, respectively, are average values each based on at least three experiments.

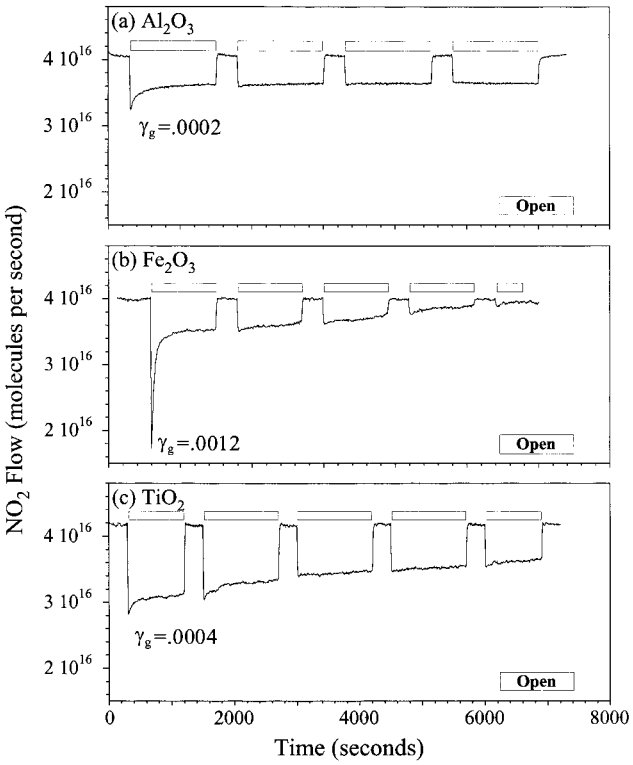

Figure 3. Knudsen cell data for the heterogeneous reaction of NO_2 on (a) Al_2O_3, (b) Fe_2O_3, and (c) TiO_2. Large sample masses between 0.5 and 2.0 g were used in these experiments. The flow rate out of the cell (molecules per second) is shown for NO_2. After a baseline flow is established, the sample compartment is opened and the NO_2 can react with the exposed oxide particles. The sample holder is then periodically closed and the NO_2 signal goes back to the baseline value. Reported values of the uptake coefficient, γ_g, are calculated using the geometric surface area of the sample and eq 2.

To ensure that our results could be extrapolated to lower concentrations the uptake coefficient as a function of NO_2 concentration was measured over a range of approximately 10 ppb to 10 ppm for Al_2O_3 particles. These data are plotted in Figure 4. From these experiments it appears that the results of this study can be extrapolated down to at least 10 ppb.

In other Knudsen cell experiments less sample was used, and in addition to monitoring NO_2 the mass spectrometer was set to monitor other mass channels including NO (*m*/*e* 30) and N_2O (*m*/*e* 44). Since NO^+ is a major fragment of NO_2 it was necessary to correct the NO signal for fragmentation from NO_2. The corrected mass spectrometer signal for NO was then converted to flow rate as described in the Experimental Section. To facilitate the direct comparison of NO produced to NO_2 reacted, the NO_2 flow data was offset by the steady-state value and inverted. In this way the number of NO_2 molecules that have reacted with the surface as well as the amount of NO produced can be plotted on the same scale (Figure 5).

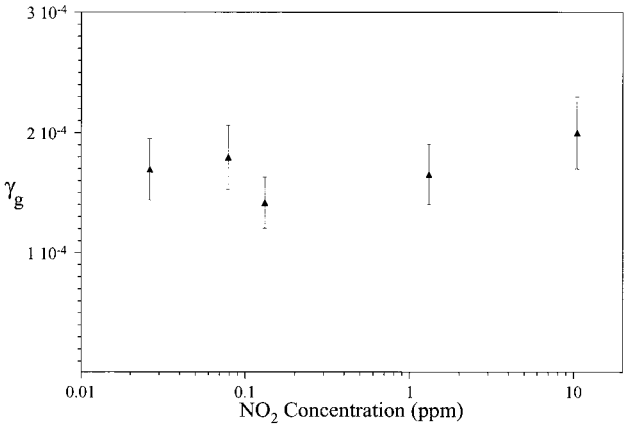

Figure 4. Uptake coefficients for NO_2 on alumina as a function of initial NO_2 concentration within the Knudsen cell. All sample masses were approximately 0.25 g. (1 ppm = 0.76 mTorr ≅ 2.4×10^{13} cm^{-3}).

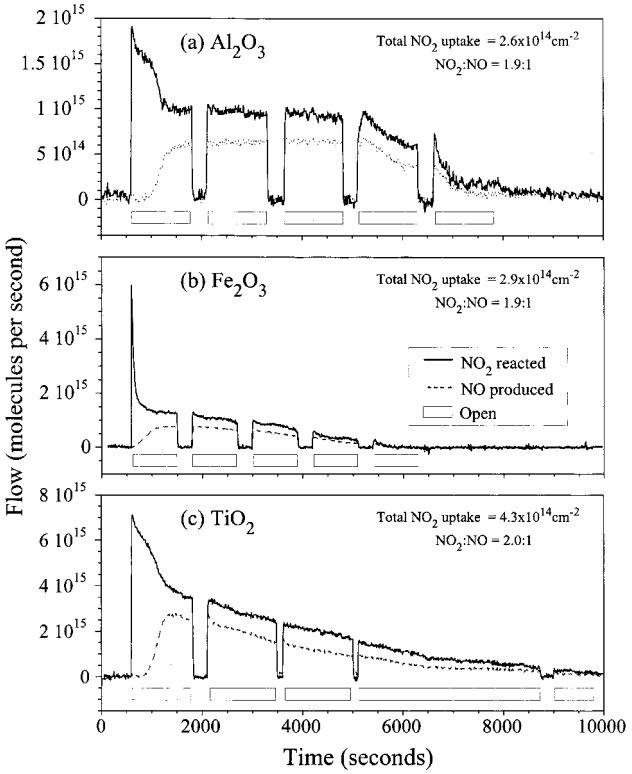

Figure 5. The flow rates of NO_2 reacted and NO produced are shown. The Al_2O_3 sample mass was 20 mg (~2660 layers), the Fe_2O_3 mass was 550 mg (~450 layers), and the TiO_2 mass was 74 mg (~6260 layers).

Several interesting and important observations can be made from the data presented in Figure 5. First, there is an induction period before the production of gas-phase NO begins. Second, by integrating the area under the curves the total number of molecules of NO_2 reacted and NO produced during the course of the experiment can be determined. For each of the oxides studied the resultant NO_2:NO ratio is very close to 2:1. In addition, by measuring the initial sample mass and knowing the BET surface area, the total number of NO_2 molecules that reacted per cm^2 can be determined for each sample. As discussed in the next section, the measured values of $(3-4) \times 10^{14}$ cm^{-2} indicate a surface nitrate coverage of around $(1.5-2) \times 10^{14}$ cm^{-2}. Perhaps most importantly, these data demonstrate that using the geometric area would give physically unreasonable values for the surface nitrate coverage ($(2-7) \times 10^{17}$ cm^{-2}). This observation provides definitive evidence that gas diffusion into the underlying layers of the oxide particles is facile.

Discussion

A. Reaction Mechanism for the Formation of Adsorbed and Gas-Phase Species from the Heterogeneous Reaction of NO_2 with Mineral Oxides. As shown here, reactions of NO_2 with the surface of mineral oxide particles result in the formation of both surface-bound and gas-phase products. Spectroscopic characterization of all the reaction products as well as coverage dependence and quantification of these products allows for a reaction mechanism to be postulated.

Initially, NO_2 reacts with the surface to form nitrite (eq 3). Nitrite can then react with either; another surface nitrite in a Langmuir−Hinshelwood (LH) type mechanism (4a), or gas-phase NO_2 in a Eley−Rideal (ER) type mechanism (4b). In either case the result is surface nitrate, which can coordinate to the surface in several different ways, and gas-phase NO. In the reactions shown below, ≡M represents a metal atom from any of the oxide surfaces.

$$NO_2(g) \rightarrow \equiv MNO_2 \quad (3)$$

$$2 \equiv MNO_2 \rightarrow \equiv MNO_3 + NO(g) \quad \text{LH} \quad (4a)$$

$$\equiv MNO_2 + NO_2(g) \rightarrow \equiv MNO_3 + NO(g) \quad \text{ER} \quad (4b)$$

Reactions 3 and 4 account for the formation of the three major products—surface nitrite, surface nitrate, and gas-phase NO.

Reactions involving the dimer, N_2O_4, e.g., $N_2O_4 \rightarrow NO^+ + NO_3^-$, have been proposed. However the delay observed prior to NO production as well as the initial appearance of surface nitrite is more consistent with the two-step mechanism depicted in reactions 3 and 4. It is important to note that nearly all previous FT-IR studies of reactions of NO_2 on metal oxide particles at 298 K did not monitor for gas-phase products.[27−32] As a result, previous mechanisms for reactions of NO_2 are based on surface-bound products only and not on a full characterization of all the reaction products.

A small amount of gas-phase N_2O (<1%), is evident in some of the FT-IR experiments. This may be the result of the reaction of the product NO with the surface of the oxides. For example, experiments preformed in our lab have shown that NO can react with TiO_2 to yield N_2O in the gas phase.[39]

B. Uptake Coefficient of NO_2 Adsorption on Mineral Oxides. The initial uptake coefficients measured for NO_2 reaction on mineral oxide particles using eq 1 lie in the $10^{-4}-10^{-3}$ range. These values are given for comparison purposes only since it is how the vast majority of uptake coefficients have been reported.[40,41] As shown here, however, gas diffusion into the underlying particle layers can readily occur and thus the true uptake coefficients for NO_2 on mineral oxides will be much lower.

There is some controversy in the literature as to whether eq 2 is appropriate for determining uptake coefficients.[11,40−46] The concern stems from the many assumptions made when the geometric surface area is used, including the assumption of a flat surface for which each gas-phase molecule that approaches the surface is either recoiled or adsorbed after only a single collision. Even assuming perfectly spherical particles and close packing, the surface morphology of a powdered sample could certainly lead to multiple collision events.[12] On the basis of a spherical, close-packed powder we estimate that the flat surface assumption will overestimate the uptake coefficient by a factor

TABLE 2: Initial Uptake Coefficients for the Reaction $NO_2(g) \rightarrow NO_2(a)$ on Oxide Particles and Parameters Used to Calculate γ_t

	symbol	Al_2O_3	Fe_2O_3	TiO_2
observed uptake coefficient	γ_g[a]	2×10^{-4}	1.2×10^{-3}	4×10^{-4}
true uptake coefficient	γ_t[b]	2×10^{-8}	7×10^{-7}	1×10^{-7}
diameter	d	1.8×10^{-6} cm	6.9×10^{-5} cm	2.5×10^{-6} cm
true density	ρ_t	3.7 g cm^{-3}	5.24 g cm^{-3}	4.17 g cm^{-3}
bulk density	ρ_b	0.15 g cm^{-3}	1.1 g cm^{-3}	0.17 g cm^{-3}
surface area	S_{BET}	1.01×10^6 cm^2 g	2.3×10^6 cm^2 g	5.0×10^6 cm^2 g
geometric area	A_s	11.88 cm^2	11.88 cm^2	11.88 cm^2
tortuosity	τ	3	3	3
external height	h_e[c]	2.1×10^{-6} cm	4.7×10^{-5} cm	3.0×10^{-6} cm
internal height	h_i[d]	5.58×10^{-3} cm	2.11×10^{-2} cm	1.88×10^{-2} cm

[a] Calculated using eq 2 and the geometric area. [b] Calculated using the diffusion model (see text for details). [c] $h_e = 0.5*(\text{particle mass}/\rho_b)^{1/3}$ = one-half the height of one layer. [d] $h_i = (\text{sample mass}/A_s\rho_b) - h_e$.

of two to three. Another and potentially far more important physical phenomena, not accounted for in the derivation of eq 2, is that of diffusion into the underlying layers.

Keyser and co-workers have developed a model that attempts to correct uptake coefficients, measured using geometric area, for the effect of bulk diffusion.[42] Their work presents a relatively complete set of justifications and derivations of the equations used in the formulation of the model; as such, the following is intended only as a brief overview.

In the model, the observed uptake coefficient, using the geometric area, γ_g, is related to the true uptake coefficient, γ_t, by eq 5:

$$\gamma_{obs} = \gamma_t (S_e + \eta S_i) \tag{5}$$

where the parenthetic term contains a correction factor for the effect of gas-phase diffusion into the underlying layers. S_e and S_i are the external and internal surface areas per unit geometric area, and η is an effectiveness factor. The effectiveness factor is essentially the fraction of the internal surface area that contributes to the measured value of the uptake coefficient. Its value can be calculated from eqs 6 and 7:

$$\eta = \frac{1}{\phi}\tanh(\phi) \tag{6}$$

$$\phi = \left(\frac{m}{\rho_b A_s d}\right)\left(\frac{3\rho_b}{\rho_t - \rho_b}\right)\left(\frac{3\tau\gamma_t}{4 - 2\gamma_t}\right)^{1/2} \tag{7}$$

where the Theile modulus, ϕ, is a measure of the relative rates of surface reaction and diffusion into the underlying layers. The value for the Theile modulus is dependent upon the samples mass, m, bulk density, ρ_b, and particle diameter, d, as well as the geometric area it occupies, A_s, and the true uptake coefficient, γ_t. A tortuosity factor, τ, is included to account for inhomogeneities in the interparticle voids. In these experiments a tortuosity factor of 3 was used in accordance with Keyser et al. The appearance of eq 7 is somewhat modified from that derived by Keyser et al. in that here we did not assume either simple cubic or hexagonal close-packing spheres. Instead the experimentally measured bulk density was used in the calculations. In addition, the specific surface area was measured rather than calculated. Rewriting eq 5 in terms of measured bulk density and BET surface area yields eq 8:

$$\gamma_{obs} = \gamma_t r_b S_{BET} (h_e + \eta h_i) \tag{8}$$

where S_{BET} is the BET specific surface area, h_e is the height of the first layer, and h_i is the height of all the internal layers calculated from the total mass, the measured bulk density, and the particle mass. Since γ_t appears in the equation for η, eq 5 must be solved iteratively. Using eq 5 and the values included in Table 2 the "true" uptake coefficients can be calculated to be 2×10^{-8} for Al_2O_3, 7×10^{-7} for Fe_2O_3, and 1×10^{-7} for TiO_2. These values, as well as those determined using the geometric surface area (eq. 2), are presented in Table 2. As explained below, although the values obtained using the model are dramatically lower than those calculated using the geometric area, the effect is not totally unexpected.

If the true value of the uptake coefficient is relatively low, then the effective diffusion constant will be higher and concomitantly the effectiveness factor will be higher. As a result the correction factor in eq 5 will approach 1.0. For thin samples, this implies that most of the BET surface area must be considered, which results in a very large correction factor. In a recent study exploring the kinetics of N_2O_5 uptake on salt, Fenter et al. found observed uptake coefficients for NaCl on the order of 10^{-2}.[41] Using the Keyser et al. model, however, they report true values of approximately 5×10^{-4}. Since the observed uptake coefficients measured here for NO_2 on oxide particles are substantially lower and the surface areas of the particles are relatively high, it is not surprising that the calculated correction factors are even greater than those for N_2O_5 on salt surfaces.

Reactions 3 and 4 indicate a net stoichiometry of two gas-phase NO_2 molecules per adsorbed nitrate as follows:

$$2NO_2(g) \rightarrow \equiv MNO_3 + NO \tag{9}$$

As a result, the total uptake of NO_2 determined here (from the data presented in Figure 5) needs to be divided by two in order to find the surface density of nitrate species. The values we calculate of $\sim 2 \times 10^{14}$ cm^{-2} support, at least qualitatively, the Keyser model; i.e., the use of some fraction of the BET surface area seems more appropriate than the use of the geometric area. However, before the model can be applied universally there are clearly more experimental considerations that will have to be addressed. First, in deriving eq 7, Knudsen diffusion was assumed. The equation for Knudsen diffusion is really just an estimate based on an elastic collision model and does not consider the "sticky" character of many species such as HNO_3.[41] A measurement of the diffusion constant for each reactant/substrate pair would help to reduce the uncertainty in the results.

Another possibility for improvement comes from the observation that the model considers only initial uptake coefficients. For these oxides, the initial uptake coefficient is a measure of reaction 3, i.e., $NO_2(g) \rightarrow NO_2(a)$. However, as the reaction proceeds, other processes come into play and the uptake coefficient is no longer a measure of eq 3 alone but also of

reactions 4a and/or 4b. The time-dependent behavior shown in Figures 3 and 5 is complex because many processes can come into play, including gas diffusion into the underlying layers and surface reaction. We are currently working on a more detailed model to mimic the time-dependent behavior of Knudsen cell data for powdered samples, and this work represents a first step in addressing some of these issues.

Conclusions

The heterogeneous reactivity of NO_2 on Al_2O_3, Fe_2O_3, and TiO_2 particles has been investigated with analytical techniques that probe both surface-bound and gas-phase products. The FT-IR data provide evidence for surface-bound nitrite (low coverage), nitrate (high coverage), and gas-phase NO. There is also some evidence for N_2O formation but this may be due to a side reaction of the NO product. The calibrated mass spectral data from the Knudsen cell experiments provide quantitative information on both the amount of NO_2 reacted and the NO produced. Initially, there is no measurable production of gas-phase species that evolve from NO_2 reaction on these oxide particles. As the surface is exposed to more NO_2 and the coverage of surface species increases, gaseous NO is formed. The initial uptake coefficients have been measured using both geometric area and a model which takes into account gas-phase diffusion into the underlying sample layers. The initial uptake coefficient is a measure of the adsorption of gas-phase NO_2 to form surface nitrite. As the reaction proceeds the measured uptake coefficient is the result of several different chemical processes and can only be described as the loss of NO_2 from the gas phase.

In a polluted environment, NO_2 concentrations can be as high as 250 ppb.[1] Reactions that alter NO_2 concentrations could alter the ratio of NO_x to HNO_3 which is of atmospheric importance due to the role that these molecules play in tropospheric ozone formation. The results of this study show that the reaction of NO_2 on mineral oxide particles in the atmosphere is likely too low to have any impact on the NO_x:HNO_3 ratio. Currently, however, measurements of heterogeneous reactions of HNO_3 on oxide surfaces show that HNO_3 is much more reactive than NO_2 on oxide particles with uptake coefficients that are nearly least 3 orders of magnitude greater than those found for the heterogeneous reaction of NO_2 on oxide particle surfaces.[46] These uptake coefficients may well be high enough to significantly impact the concentration of HNO_3 in the atmosphere.

Acknowledgment. The authors gratefully acknowledge the National Science Foundation (Grant CHE-9614134) as well as the Camille and Henry Dreyfus Postdoctoral Program in Environmental Chemistry for support of this research. The authors thank Angela Goodman for the TEM measurements of the oxide particles.

References and Notes

(1) Seinfeld, J. H. *Atmospheric Chemistry and Physics of Air Pollution*; Wiley: New York, 1986.
(2) Sillman, S.; Logan, J. A.; Wofsy, S. C. *J. Geophys. Res.* **1990**, *95*, 1837−1851.
(3) Chatfield, R. B. *Geophys. Res. Lett.* **1994**, *21*, 2705.
(4) Hauglustain, D. A.; Ridley, B. A.; Solomon, S.; Hess, P. G.; Madronich, S. *Geophys. Res. Lett.* **1996**, *23*, 2069.
(5) Rogaski, C. A.; Golden, D. M.; Williams, L. R. *Geophys. Res. Lett.* **1997**, *24*, 381.
(6) Tabor, K.; Gutzwiller, L.; Rossi, M. J. *J. Phys. Chem.* **1994**, *98*, 6172.
(7) Kalberer, M.; Tabor, K.; Ammann, M.; Parrat, Y.; Weingartner, E.; Piguet, D.; Jost, D. T.; Turler, A.; Gaggeler, H. W.; Baltensperger, U. *J. Phys. Chem.* **1996**, *100*, 15487.
(8) Amman, M.; Kalberer, M.; Jost, D. T.; Tobler, L.; Rossler, E.; Piguet, D.; Gaggeler, H. W.; Baltensperger, U. *Nature* **1998**, *395*, 157.
(9) Gerecke, A.; Thielmann, A.; Gutzwiller, L.; Rossi, M. J. *Geophys. Res. Lett*. **1998**, *25*, 2453.
(10) Lary, D. J.; Lee, A. M.; Toumi, R.; Newchurch, M. J.; Pirre, M. *J. Geophys. Res.* **1997**, *102* (D3), 3671.
(11) Longfellow, C. A.; Ravishankara, A. R.; Hanson D. R. *J. Geophys. Res.* **1999**, in press.
(12) Beichert, P.; Finlayson-Pitts, B. J. *J. Phys. Chem.* **1996**, *100*, 15218.
(13) Vogt, R.; Finlayson-Pitts, B. J. *Geophys. Res. Lett*. **1994**, 2291.
(14) Vogt, R.; Finlayson-Pitts, B. J. *J. Phys. Chem.* **1994**, *98*, 3747.
(15) Kutsunaand, S.; Ibuski, T. *J. Geophys. Res.* **1994**, *99*, 25479.
(16) Peters, S. J.; Ewing, G. E. *J. Phys. Chem*. **1996**, *100*, 14093.
(17) Leu, M. T.; Timonen, R. S.; Keyser, L. F., Yung, Y. L. *J. Phys. Chem.* **1995**, *99*, 13203.
(18) Junkermann, W.; Ibuski, T. *Atmos. Environ.* **1992**, *26A*, 3099.
(19) Dentener, F. J.; Crutzen, P. J. *J. Geophys. Res.* **1993**, *98* (D4), 7149.
(20) Dentener, F.; Carmichael, G.; Zhang, Y.; Lelifeld, J.; Crutzen., P. *J. Geophys. Res.* **1996**, *101* (D17), 22, 869.
(21) Zhang, Y.; Sunwoo, Y.; Kotamarthi, V.; Carmichael, G. *J. Appl. Meteorol.* **1994**, *33*, 813.
(22) Mamane, Y.; Gottlieb, J. *J. Aerosol Sci.* **1990**, *21*, S225.
(23) Miller, T. M.; Grassian, V. H. *J. Am. Chem. Soc.* **1995**, *117*, 10969.
(24) Goodman, A. L.; Miller, T. M.; Grassian, V. H. *J. Vac. Sci. Technol., A* **1998**, *16*, 2585.
(25) Bickley, R. I.; Gonzalez-Carreno, T.; Lees, J. S.; Palmisano, L.; Tilley, R. J. D. *J. Solid State Chem.* **1991**, *92*, 178.
(26) Dushman, S. *Scientific Foundations of Vacuum Technique*, 2nd ed.; Wiley: New York, 1962.
(27) Pozdnyakov, D. V.; Filimonov, V. N. *Kinet. Katal.* **1973**, *14*, 760.
(28) Hadjiivanov, K.; Bushev, V.; Kantcheva, M.; Klissurski, D. *Langmuir* **1994**, *10*, 464.
(29) Stark, J. V.; Klabunde, K. J. *Chem. Mater.* **1996**, *8*, 1913.
(30) Hadjiivanov, K. I.; Klissurski, D. G.; Bushev, V. P. *J. Chem. Soc., Faraday Trans.*, **1995**, *91* (1), 149.
(31) Busca, G.; Lorenzelli, V. *J. Catal.* **1981**, *72*, 303.
(32) Navio, J. A.; Cerrillos, C.; Real, C. *Surf. Interface Anal.* **1996**, *24*, 355.
(33) Nakamoto, K. *Infrared Spectra of Inorganic and Coordination Compounds*; Wiley: New York, 1970.
(34) Hitchman, M. A.; Rowbottom, G. L. *Coord. Chem. Rev.* **1982**, *42*, 55−132.
(35) Davydov, A. A. *Infrared Spectroscopy of Adsorbed Species on the Surface of Transition Metal Oxides*; Wiley and Sons: Chichester, 1990.
(36) Suda, Y.; Morimoto, T. *Langmuir* **1987**, *3*, 786.
(37) Miller, T. M.; Grassian, V. H. *Geophys. Res. Lett*. **1998**, *25*, 3835.
(38) Golden, D. M.; Spokes, G. N.; Benson, S. W. *Angew Chem., Int. Ed. Engl*. **1973**, *12*, 534.
(39) Goodman, A. L.; Grassian, V. H. Unpublished results.
(40) DeMore, W. B.; Sander, S. P.; Golden, D. M.; Hampson, R. F.; Kurylo, M. J.; Howard, C. J.; Ravishankara, A. R.; Kolb, C. E.; Molina, M. J. *Chemical Kinetics and Photochemical Data for Use in Stratospheric Modeling*; JPL publication 97-4, 1997.
(41) Fenter, F. F.; Caloz, F.; Rossi, M. J. *J. Phys. Chem.* **1996**, *100*, 1008.
(42) Keyser, L. F.; Moore, S. B.; Leu, M. T. *J. Phys. Chem.* **1991**, *95*, 5496.
(43) Hanson, D. R.; Ravishankara, A. R. *J. Phys. Chem.* **1992**, *96*, 2682.
(44) Keyser, Leon F.; Leu, M.-T.; Moore, S. B. *J. Phys. Chem.* **1993**, *97*, 2800.
(45) Leu, M.-T.; Timonen, R. S.; Keyser, L. F.; Yuk, L. Y. *J. Phys. Chem.* **1995**, *99*, 13203.
(46) Underwood, G. M.; Grassian, V. H. Unpublished results.